Hindawi
Shock and Vibration
Volume 2021, Article ID 6653390, 13 pages
https://doi.org/10.1155/2021/6653390

Research Article

Design Optimization and Performance Analysis of the Pneumatic DTH Hammer with Self-Propelled Round Bit

Kun Bo,[1,2] Siyuan Sun,[1,2] Yong Hu,[3] and Maosen Wang [1,2]

[1]*College of Construction Engineering, Jilin University, Changchun 130021, China*
[2]*Key Laboratory of Ministry of Natural Resources on Complicated Conditions Drilling Technology, Jilin University, Changchun 130021, China*
[3]*School of Mechanical and Aerospace Engineering, Jilin University, Changchun 130025, China*

Correspondence should be addressed to Maosen Wang; wangms@jlu.edu.cn

Received 30 November 2020; Revised 8 June 2021; Accepted 25 June 2021; Published 6 July 2021

Academic Editor: Ling Zhou

Although pneumatic down-the-hole (DTH) hammers have good performance of high penetration rate and minimal deviation tendency in the vertical section of oil and gas wells, they have not been successfully used in directional drilling due to drill tool wear and wellbore disturbance. Herein, we developed a novel type of pneumatic DTH hammer with a self-propelled round bit to overcome the technical difficulties of directional drilling. Nonlinear dynamic modeling developed by the authors was used to analyze the working principle and performance of the novel DTH hammer. The kinematics and dynamics simulation of this hammer were carried out using MATLAB language, and the motion law of the piston was revealed. The performance of the novel hammer was numerically simulated and evaluated by considering fluctuations of the front and rear chamber pressure, impact energy, acceleration, and frequency. The results show that our novel DTH hammer's working principle is feasible and has an adequate structural design. The simulation results demonstrate reasonable design parameters. Compared to the numerical results for conventional DTH hammers, the velocity and acceleration of the piston of the novel hammer changed smoothly. The frequency was slightly higher than that of conventional hammers, while other parameters were nearly equal. The novel DTH hammer can be used in directional drilling, trenchless drilling, and seabed sampling drilling.

1. Introduction

Pneumatic DTH hammer drilling is a rotary percussive drilling technique widely used in many fields, such as open-pit mines [1], geological core exploration [2], and petroleum exploration [3]. The existing pneumatic hammer drilling technology has many advantages: high drilling efficiency, excellent bit lift, and good hole quality [4–7]. In conventional DTH hammer drilling, the hammer is fixed at the bottom of the drill string that has the primary function of providing rotational torque and axial pressure. The hammer driven by compressed air transforms the inner energy into the kinetic energy of the piston, and the impact energy is transmitted to the bit in the form of stress wave for rock breaking. Meanwhile, the rotational torque rotates the bit to tear and cut rock.

Many scholars have performed theoretical and experimental research on the improvement of pneumatic DTH hammers. Ryu et al. [8] developed a novel technique for micro-tunnel excavation using a multihammer drilling machine and identified the optimum operating conditions of the system. Bu et al. [9, 10] studied the phenomenon of the drill string's axial forced vibration with a periodic impacting force under DTH drilling in an innovative manner. Depouhon et al. [11] presented a novel dynamical model to analyze the long-term response of the percussive drilling system. They subsequently used a low-dimension model to study the process of percussive drilling [12]. Chiang and Stamm [13] presented a nonlinear dynamic model to compute the hammer performance, and the results were in agreement with the predicted values. Eremenko et al. [14] determined the causes of performance drop in induced block

caving using fans of two types of the hammer and discussed alternatives of improvement in drilling efficiency. Kim et al. [15, 16] developed a pneumatic dynamic model of DTH hammer to predict drilling performance and validated the model through laboratory tests. The application of the DTH hammer in the vertical section of oil fields has shown that its penetration rate is several times that of conventional rotary drilling. However, many technical problems persist in using a DTH hammer for directional wells and horizontal wells, such as greater friction and rotary table driving difficulty. The gas screw cannot drive the air hammer due to a low-pressure drop and other issues, especially the issue that friction force consumes a tremendous amount of energy imparted to the drilling string. This often generates torsional vibration [3]. The authoritative publication *Air and Gas Drilling Manual* states that pneumatic DTH hammer has only been applied in vertical drilling. Zhao et al. [17] verified that the adequate power and drilling rate would decline with the increase of devotion angle.

Nowadays, since conventional DTH hammers have a well-tried structure, their modified versions were designed to solve the above problems. Klishin et al. [18] created an elastic valve to enhance the air hammer's energy performance and drilling durability in directional drilling. Liu and He [19, 20] designed a novel rotation air hammer and used the LS-DYNA program to analyze the impact dynamics problem of its piston and drill bit to obtain their stress change rule in the impact process. The present article introduces a novel DTH hammer and describes its working principle and design method. This hammer inherits the pneumatic hammer's advantages, adequately utilizes the energy of the returning stroke of the piston, and achieves a self-propelled round of the bit [21]. Furthermore, we redesigned the air distributor, a special-purpose piston, and the rotation joint. The ratchet wheel mechanism is also introduced to realize the separate motions of the drill pipe and the bit.

2. Mechanical Structure and Working Principle

2.1. Structure Design. The structure of the novel pneumatic DTH hammer with a self-propelled round bit is shown in Figure 1. The impact mechanism and rotation mechanism are included in the hammer that is driven by compressed air. The impact mechanism mainly consists of a valve, air distributor, inner cylinder, and piston. The rotation mechanism primarily involves a spiral rod, piston (with the rear ends equipped with a spiral nut), rotary joint, connector, and ratchet wheel mechanism (Figure 2). The head of the spiral rod is equipped with pawls, and the tail ties in with a spiral nut. These pawls support the internal teeth of the ratchet under the force of a tower-shaped spring. The ratchet wheel and the air distributor are designed into a single part.

In the strike stage, compressed air is delivered from the air compressor through the push valve, and it flows into the rear chamber through the distributor and the inner cylinder. The piston travels down in a straight line with high speed under the action of pressure difference. Since the spiral nut fixed in the rear end of the piston is in a splined joint with the spiral rod, the latter connected with the ratchet wheel mechanism will rotate clockwise to a certain degree while the spiral nut is going down with the piston. At this moment, the pawls fixed on the head of the spiral rod are turning along with the ratchet wheel, and the spiral rod is in idling condition. The hammer casing and the bit are in the nonrotating stage.

In the backhaul stage, compressed air will get into the top sub to open the valve and flow into the front chamber, i.e., from distributor to inner cylinder. Then, the piston makes a return strike under the pressure differential. Meanwhile, the spiral rod connected with the ratchet wheel mechanism rotates counterclockwise to a certain degree, and the pawls hold the internal teeth of the ratchet wheel. When the helical moment of the spiral rod is sufficient enough to overcome the resistance moment of the hammer case and rocks, pawls on the spiral rod drive the ratchet wheel to move and make it rotate with the spiral rod to a certain degree. As the ratchet wheel is in a threaded joint with the hammer case, and the hammer case is in a splined joint with the drill bit, it is easy to make the hammer case drive the drill bit to rotate simultaneously and realize self-propelled round motion.

The most distinguishing characteristic of the proposed hammer is the self-propelled round mechanism. When compressed air flows into the hammer, the drill bit can rotate driven by the hammer casing, while the drill pipe is static without a drilling rig. Due to the drill pipe being stationary in this hammer design, the quality of the wellbore and stiffness of the drill pipe will be improved, and the efficiency of breaking rocks will increase, thus having a great significance to directional drilling in construction engineering applications.

2.2. Working Principle of the DTH Hammer. During the reciprocating linear motion of the piston, the front and rear chambers will go through the intake phase, expansion (compression) phase, and exhaust phase. The working principle of the DTH hammer is briefly shown in Figure 3 [22]. In the following sections, a dynamic model derived for the DTH hammer is constructed and used for a design optimization methodology based on a secant approximation to the gradient of space of design variables, which allows searching for an optimal solution.

As shown in Figure 3(a) and Table 1, compressed air flows into the front chamber at the initial stage, and the piston moves backward; air in the rear chamber is exhausted to the bottom hole. When the displacement of piston is between the L_5 and L_3 (stage b), air in the rear chamber begins to be compressed due to the closed rear exhaust channel. At stage c ($L_3 \le L < L_4$), when the upper surface of the midstep of the piston reaches the lower surface of the inner cylinder, the front intake channel is closed, and air in the front chamber starts to expand, pushing the piston continuously backward. At stage d ($L_4 \le L < L_2$), when the lower surface of the rear step of the piston reaches the lower surface of the inner cylinder

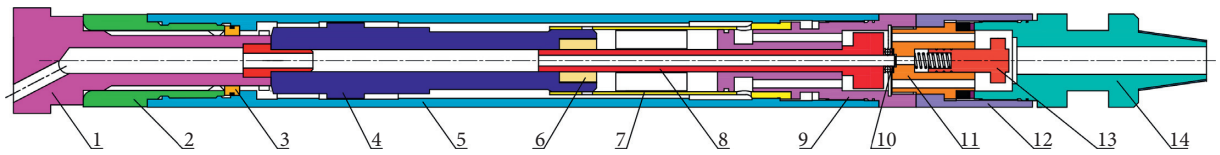

Figure 1: Main parts of the pneumatic DTH hammer with the self-propelled round bit: 1, drill bit; 2, driver sub; 3, bit retainer ring; 4, piston; 5, hammer casing; 6, spiral nut; 7, inner cylinder; 8, spiral rod; 9, air distributor; 10, thrust ball bearing; 11, rotary joint; 12, connector; 13, valve; 14, top sub.

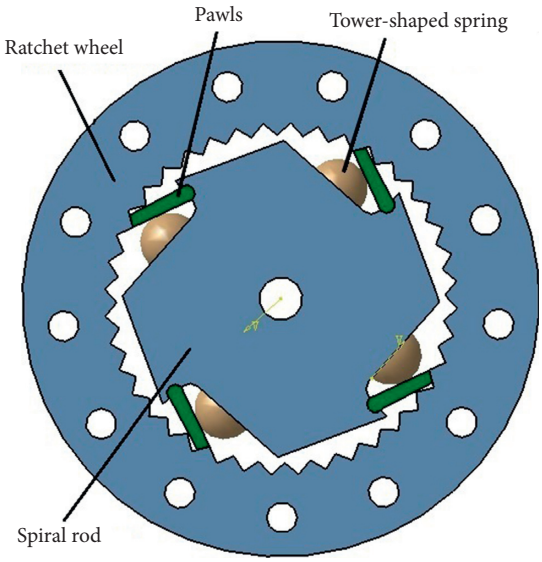

Figure 2: Structure diagram of the ratchet wheel mechanism.

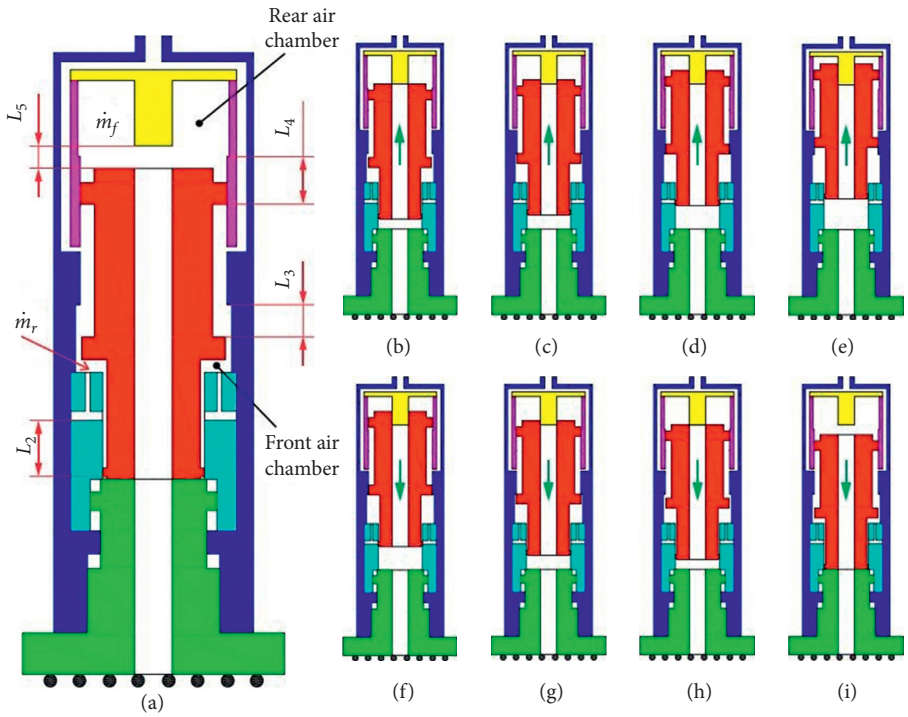

Figure 3: Schematic of the pneumatic DTH hammer.

Table 1: Air condition and bit motion at each stage.

Stage	Displacement of the piston (L)	Air condition (front chamber)	Air condition (rear chamber)	Piston motion	Bit motion
a	$0 \le L < L_5$	Air intake ($\dot{m}_f > 0$)	Air exhaust ($\dot{m}_r < 0$)	Backhaul stage	Rotation
b	$L_5 \le L < L_3$	Air intake ($\dot{m}_f > 0$)	Air compression ($\dot{m}_r = 0$)	Backhaul stage	Rotation
c	$L_3 \le L < L_4$	Air expansion ($\dot{m}_f = 0$)	Air compression ($\dot{m}_r = 0$)	Backhaul stage	Rotation
d	$L_4 \le L < L_2$	Air expansion ($\dot{m}_f = 0$)	Air intake ($\dot{m}_r > 0$)	Backhaul stage	Rotation
e	$L_2 \le L \le L_1$	Air exhaust ($\dot{m}_f < 0$)	Air intake ($\dot{m}_r > 0$)	Backhaul stage	Rotation
f	$L_4 \le L < L_2$	Air compression ($\dot{m}_f = 0$)	Air intake ($\dot{m}_r > 0$)	Strike stage	Nonrotation
g	$L_3 \le L < L_4$	Air compression ($\dot{m}_f = 0$)	Air expansion ($\dot{m}_r = 0$)	Strike stage	Nonrotation
h	$L_5 \le L < L_3$	Air intake ($\dot{m}_f > 0$)	Air expansion ($\dot{m}_r = 0$)	Strike stage	Nonrotation
i	$0 \le L < L_5$	Air intake ($\dot{m}_f > 0$)	Air exhaust ($\dot{m}_r < 0$)	Strike stage	Nonrotation

L_5, L_3, L_4, and L_2 represent a specific key location of the piston where the air conditions change at each stage, especially L_1 representing the piston's actual strike. $\dot{m}_f$ and $\dot{m}_r$ represent the instantaneous mass flow rate passing through the front chamber and the rear chamber (Figure 3), respectively.

groove, compressed air flows into the rear chamber and generates an opposite force acting on the piston, so that the backward motion of piston begins to slow down. Stage e is a particular condition where the air in the front chamber is exhausted, and the piston stops at L_1. Under the push force of compressed air in the rear chamber, the velocity of piston becomes zero. Throughout the above procedure, high kinetic energy moves backward, driving the spiral rod rotation. The ratchet on the spiral rod moves the ratchet wheel to drive the hammer case and the drill bit to rotate together, realizing the self-rotational movement of the bit. After a motion direction change at stage e, the piston is accelerated forward to the drill bit. The conditions of air at stages f, g, h, and i are similar to the above stages of a to e.

3. Numerical Simulation

3.1. Modeling of the Pneumatic DTH Hammer. The mathematical modeling of the DTH hammer is mainly based on a one-dimensional gas flow equation of state, energy conservation equation, continuous equation in the front and rear chambers, and piston motion differential equation [23–25]. The piston movement distance can be calculated by selecting the time step, and the state parameters in each time step can be regarded as those in a quasi-static process (Figure 4).

As shown in Figure 4, the piston is a vital component in the operating mechanism of the pneumatic DTH hammer. Therefore, the corresponding mathematical models were established based on the ideal gas law:

$$P_i V_i = M_i R T_i, \tag{1}$$

where P_i, M_i, and T_i denote the absolute press, gas mass, and absolute temperature in the front and rear chamber, respectively; V_i denotes the front and rear chamber volume; and R is the ideal gas constant.

When there is gas exchange between the chamber and the outside, the influence of gas mass must be considered; thus, the energy equation of the chamber can be expressed as

$$\mathrm{d}Q + \mathrm{d}M_i = \mathrm{d}U + \mathrm{d}W + \mathrm{d}M_o. \tag{2}$$

Assuming that there is no heat exchange between the gas in the chamber and the outside during piston motion, then $\mathrm{d}Q = 0$. In the equation, $\mathrm{d}M_i$ denotes the kinetic energy of inflow, $\mathrm{d}U$ denotes the internal energy of the gas in the chamber, $\mathrm{d}M_0$ denotes the kinetic energy of the outflow, and $\mathrm{d}W$ indicates the work of gas expansion.

The gas volume change in the front and rear chambers is given by

$$V^{n+1} = V^n + \frac{\mathrm{d}V}{\mathrm{d}t}\Delta t, \tag{3}$$

where n and $n+1$ represent the respective quantity at the current and following time step values; for example, V^{n+1} denotes the volume of the chamber at $(n+1)$th time step.

$$\mathrm{d}P = \frac{K}{V}\left(RT_0\mathrm{d}M - P\mathrm{d}V\right). \tag{4}$$

Considering the relationship between specific heat at constant volume C_p, specific heat at constant volume C_v, and adiabatic index K of the ideal gas, the variation of gas pressure at any time step is given as

$$\mathrm{d}P = \frac{K}{V}\left(RT_0\mathrm{d}M - P\mathrm{d}V\right), \tag{5}$$

where V denotes the volume of the front and rear chamber, T_0 is the absolute temperature of gas, $\mathrm{d}M$ denotes the variation of gas mass in the chamber, and $\mathrm{d}V$ denotes the variation of volume in the chamber.

The variation of gas temperature at any time step is expressed as

$$\mathrm{d}T = \frac{T}{V}\cdot\frac{R}{P}\left[(K-1)T_0\mathrm{d}M\right] - \frac{K-1}{V}T - \mathrm{d}V. \tag{6}$$

When determining the mass flow rate in the front and rear chambers, we should first calculate the gas velocity passing through the exhaust port and then choose the corresponding calculation formula. The critical pressure ratio ζ determines the type of sound speed:

$$\zeta = \frac{P_{ci}}{P_{co}} = \left(\frac{2}{K+1}\right)^{K/(K+1)}. \tag{7}$$

When $P_{ci}/P_{co} > \zeta$, the gas velocity is less than the acoustic velocity and is equivalent to subsonic speed. The mass flow rate in the chamber is then calculated as follows:

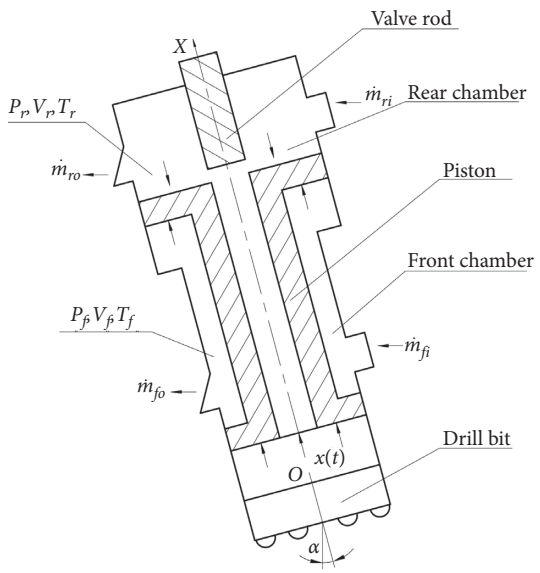

Figure 4: Mathematical schematics of the DTH hammer.

$$\dot{m} = A \cdot \eta \cdot P_{co} \cdot \sqrt{\frac{2}{R \cdot T_i}\left(\frac{K}{K+1}\right) \cdot \left[\left(\frac{P_{ci}}{P_{co}}\right)^{2/K} - \left(\frac{P_{ci}}{P_{co}}\right)^{(K+1)/K}\right]}. \tag{8}$$

When $P_{ci}/P_{co} \le \zeta$, the gas velocity is equal to or more than the acoustic velocity and is equivalent to critical rate and subsonic speed. The mass flow rate in the chamber is then calculated as follows:

$$\dot{m} = A \cdot \eta \cdot P_{co} \sqrt{\frac{K}{R \cdot T_i}\left(\frac{2}{K+1}\right)^{(K+1/K-1)}}, \tag{9}$$

where P_{ci} and P_{co} denote the air pressure at the inlet and outlet of the chamber, respectively; K represents the adiabatic index of gas and $K = 1.4$; T_i indicates the downstream airflow temperature; A means the section area of the flow channel; and η is the resistance coefficient of gas flow.

The coordination of the DTH hammer is shown in Figure 4. The coordination origin of the piston is at the end of the front chamber, and the upward motion is positive when the front face of the piston is in contact with the upper face of the bit; V_{f0} and V_{r0}, respectively, denote the front and rear chamber's initial volume.

Force acting on the piston mainly consists of gravity and pressure-induced forces. The friction force is sufficiently low and is ignored in the modeling process. The acceleration equation of the piston is given by Newton's second law as follows:

$$a = \frac{\mathrm{d}^2 X}{\mathrm{d}t^2} = \frac{1}{M}\left(P_f A_f - P_r A_r + P_c A_b\right) - g \cos \alpha, \tag{10}$$

where P_f and P_r, respectively, denote the gas pressure in the front and rear chambers; P_c denotes the backpressure in the borehole; A_f and A_r denote the effective area of the piston in front and rear chambers, respectively; and A_b denotes the area of the front surface of the piston. In addition, g represents the acceleration of gravity ($g = 9.81\ \mathrm{m/s^2}$), α represents the angle of inclination, and M is the mass of the piston.

The motion equations of the piston can be determined by selecting the time step, and the state parameters in each time step can be regarded as those of a quasi-static process. When the piston makes a reciprocating motion, the velocity v^{n+1} of the piston at the $(n+1)$th time step can be calculated as

$$v^{n+1} = \frac{\mathrm{d}X}{\mathrm{d}t} = v^n + a^n \Delta t, \tag{11}$$

where a^n denotes the piston acceleration at the $(n+1)$th time step.

Furthermore, the displacement X^{n+1} of the piston at the $(n+1)$th time step is calculated as follows:

$$X^{n+1} = X^n + v^n \Delta t + \frac{1}{2} a^n \Delta t^2. \tag{12}$$

All of the working parameters of the DTH hammer depend on the motion parameters of the piston and the physical gas parameters in the front and rear chamber. They are calculated based on the above integral equations.

The impact energy of the hammer is calculated by

$$E = \frac{1}{2} m v_{\mathrm{end}}^2. \tag{13}$$

The frequency of the hammer is calculated by

$$f = \frac{1}{T_s}. \tag{14}$$

The air consumption of the hammer is calculated by

$$Q = k \bullet f \bullet \left[\sum_{i=1}^{n}\left(\dot{m}_{fo} + \dot{m}_{ro}\right) \bullet \frac{\Delta t}{\rho_0}\right], \tag{15}$$

where m denotes the piston mass; V_{end} denotes the final impact velocity of the piston; T_s denotes the motion cycle of the piston; k denotes the flow rate coefficient; $\dot{m}_{fo}$ represents the mass flow rate of the outlet in the front chamber; $\dot{m}_{ro}$ denotes the mass flow rate of the outlet in the rear chamber; Δt denotes the time step; and ρ_0 denotes the free gas density.

The torque of the self-propelled DTH hammer is used to overcome the moment of resistance force of rock acting on the bit and the hammer case during drilling. Torque is also one of the leading technical parameters of the DTH hammer and can be calculated by

$$M_T = \frac{1}{2} K_M r F_r P_0 \tan(\alpha - \varphi), \tag{16}$$

where r denotes the average diameter of the spatial rod; α denotes helix angle; φ denotes the friction angle of the screw pair; K_M denotes torque coefficient, and $K_M = 0.3$~0.4; P_0 denotes the pressure; and F_r denotes the effective section area of the piston during the backhaul stage.

There is backhaul motion of the piston drive during the rotary motion of the drill bit through the ratchet wheel mechanism, and the resistance of the piston during the backhaul stage can be calculated by

$$F_c = \frac{2}{r} \bullet \frac{M_T}{\tan(\alpha - \varphi)}. \quad (17)$$

3.2. Numerical Methodology. Based on the pneumatic DTH hammer modeling process, the method of solving the numerical integration was used to simulate the kinematics and dynamics of the piston. In the engineering simulation, the Runge–Kutta method has rigorous mathematical derivation power and high calculation accuracy. Therefore, this method was selected as the computer simulation analysis method of the DTH hammer with a self-propelled round bit.

The basic principle of the Runge–Kutta method is to use the linear combination of $f(x, y)$ values at some points to construct a kind of calculation formula. The expression of fourth-order in the Runge–Kutta method is as follows:

$$\begin{cases} y_{n+1} = y_n + \dfrac{(k + 2k_2 + 2k_3 + k_4)}{2}, \\ k_1 = hf(x_n, y_n), \\ k_2 = hf\left(x_n + \dfrac{h}{2}, y_n + \dfrac{k_1}{2}\right), \\ k_3 = hf\left(x_n + \dfrac{h}{2}, y_n + \dfrac{k_2}{2}\right), \\ h_4 = hf(x_n + h, y_n + k_3). \end{cases} \quad (18)$$

In theoretical modeling, the motion process of the piston and rotary assembly was divided into several steps, and the boundary conditions were invariant in each step. The differential equation of gas flow was established according to the boundary conditions. The fourth-order Runge–Kutta method was used to solve the differential equation. We adopted MATLAB language to calculate the differential equation of each stage of the hammer and obtain the piston and rotary assembly motion in each step.

Firstly, the subroutine *m* function file was built according to the modeling of each stage. In order to facilitate the assignment of initial conditions, the initial state also formed an independent file, and the judgment conditions of changes between each stage were unified in the main routine file. The latter was used to call the subroutine to solve the differential equations of each step and then obtain the calculation results.

For each stage, there were two main tasks to be carried out. One was to choose the calculation formula and calculate the gas flow rate in the unit time step according to the type of gas flow. Another was to calculate the pressure in chambers and determine the force of the piston at each time step of the strike and backhaul stage according to pressure change, volume change, and temperature change in the front and rear chambers. The motion law, air consumption, and pressure change of piston and rotary assembly were determined through iterative calculation. The technical parameters of the hammer, such as impact energy, impact frequency, air consumption, and required pressure, were finally obtained.

4. Experiment Validation of Structural Design

Figure 5 depicts a schematic of the test device, which consists of several components: mainframe, air compressor, DTH hammer, data acquisition system, and rocks. We executed a series of experiments to study the working behavior and to verify the rationality of the proposed mechanical design. This test device, driven by chains, can adjust the inclination of the mainframe from 0° to 90°. The hammer can be controlled at constant angular velocity and extrusion force by a geared brushless servomotor and chain mechanism. The air supplied by a compressor is infused through the motor and enters the hammer via a short drill rod joint.

A pressure transducer installed at the gas injection port was used to measure the inlet pressure. A photoelectric whirl measuring apparatus recorded the angular velocity of the hammer. In order to accurately establish the motion law of the piston, an acceleration transducer was embedded in the inner surface of the piston. This transducer can record the motion of the piston under varying conditions of different working pressures, such as velocity, acceleration, displacement, and impact frequency. All of the experimental data captured by high-speed data acquisition are used to precisely record and analyze the operational status of the hammer.

Under working pressure, the novel hammer can perform regular working cycles, and the self-rotating motion of the drill bit is realized during the backhaul stage. The acceleration transducer can measure the movement of the piston and record some data. Based on the displacement curve and velocity curve (shown in Figures 6 and 7), we can analyze the motion laws of the piston and determine technical parameters such as velocity and frequency. The experimental data are generally smaller than the simulation data, though the error is still within the allowable range (Table 2).

5. Results and Discussion

As shown in Table 3, the initial conditions of simulation are input into the calculation program. The numerical simulation can accurately express the gas state parameters in the front and rear chamber at any time step. These parameters include the position, velocity, and acceleration of the piston and other working parameters such as frequency, impact energy, and air consumption. According to the simulation results, the rationality of the design scheme can be analyzed, and the structure of the hammer can be further improved.

5.1. Simulation of Pressure Change in the Chamber. Figures 8 and 9 show the change of air pressure in the front and rear chambers in an approximate impact period. In the backhaul stage, the pressure increases rapidly in the front chamber during its air intake process ($0 < L < L_3$). With the closure of the rear chamber, its pressure increases while the rate of pressure growth decreases. When the pressure rises to a certain level, the rear chamber enters a closed state, and its

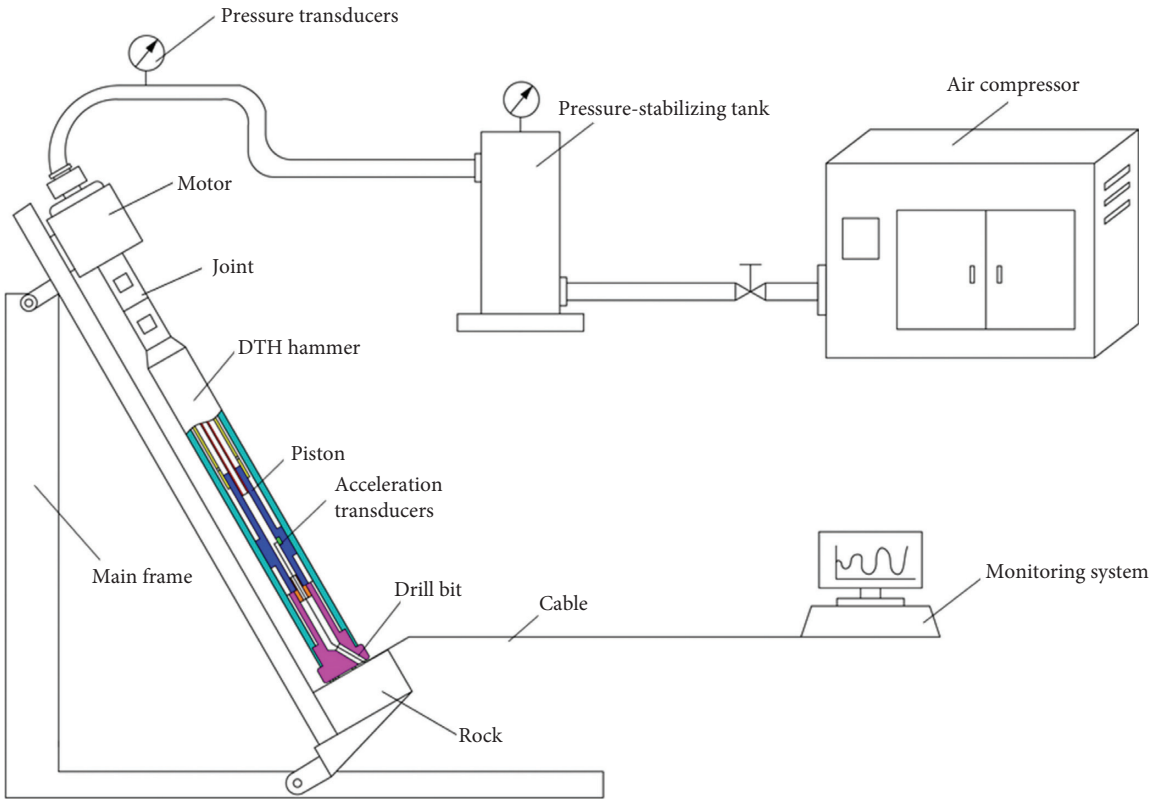

Figure 5: Schematic view of the multifunctional pneumatic hammer test device.

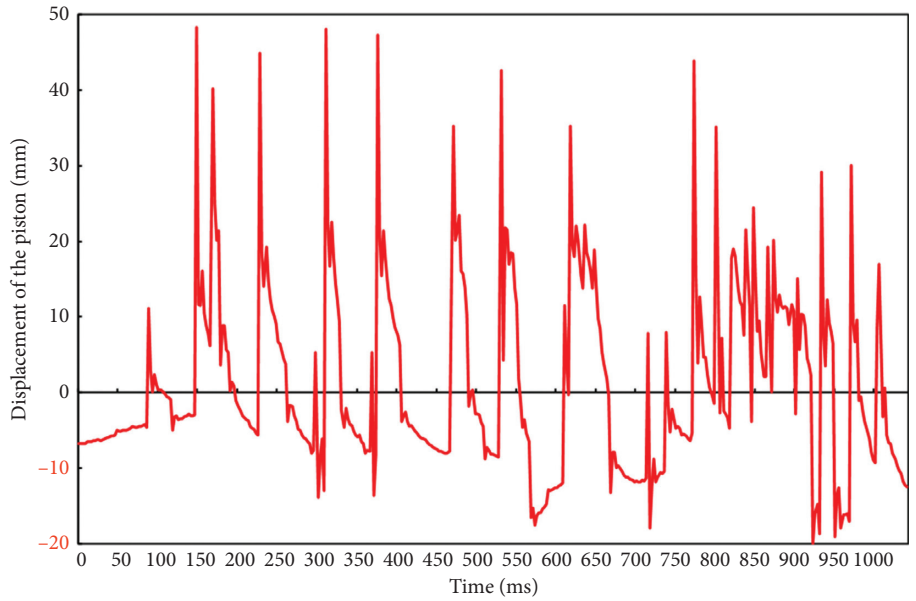

Figure 6: Impact piston displacement curve.

pressure increases. The compressed air entering the front chamber gradually decreases and tends to stabilize at 0.32 MPa.

During the expansion process of the front chamber ($L_3 < L < L_2$), the pressure increases with the volume due to the reduced airtight front chamber space. During the exhaust process of the front chamber ($L_2 < L < L_1$), the pressure continues to decrease with the change of volume. At the same time, due to the start of the exhaust stage, this dual effect decreases the front chamber pressure opposite to an increasing one.

Once the piston has moved to the top dead center position ($L = L_1$), it enters the strike stage. During air exhaust ($L_2 < L < L_1$), the front chamber's volume decreases, and its

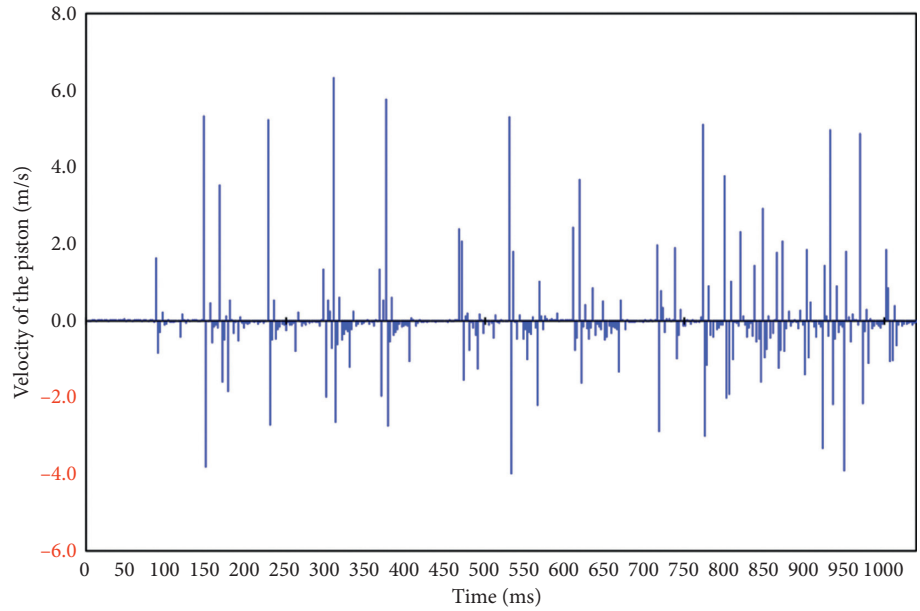

Figure 7: Impact piston velocity curve.

Table 2: Comparison of results between measurement and simulation.

	Displacement (mm)	Impact velocity (m/s)	Frequency (Hz)	Impact energy (J)
Measurement	60	5.8	24	67.3
Simulation	62	6.2	28	76.1
Error (%)	3.33	6.89	7.69	13.07

Table 3: Initial condition of simulation.

Hammer diameter (mm)	Piston mass (kg)	Air pressure (MPa)	Air flow rate (m^3/min)	Resistant force (N)
Φ105	4	1.2	5	Strike stage: 100 Backhaul stage: 50

pressure increases, but these pressure changes are minimal. During the front chamber compression process ($L_3 < L < L_2$), the pressure rises with volume reduction. During the progress of air intake ($0 < L < L_3$), due to the continuous airflow and volume reduction, the trend of pressure rise becomes stronger. The changing direction of pressure in the rear chamber will be opposite to that in the front chamber. At the end of the backhaul stage, the volume of the rear chamber is the smallest, and the pressure reaches the maximum value of 1.2 MPa.

5.2. Simulation of Piston Acceleration. Figures 10 and 11 show the acceleration change of the piston in an approximate impact period. During the backhaul stage, at the exhaust stage of the rear chamber ($0 < L < L_5$), the acceleration initially shows a sharp rise due to the rapid growth of pressure difference between the front and rear chambers. Subsequently, the pressure of the front chamber changes a little, and the acceleration curve becomes stable. At the process of $L_3 < L < L_2$, the acceleration increases firstly and then decreases, while the range of this change is relatively small. In the $L_2 < L < L_1$ stage, the gas pressure of the front chamber quickly drops, and that in the rear chamber tends to stabilize. Thus, the acceleration drop intensifies again until the end of the backhaul period.

5.3. Simulation of Piston Motion. As shown in Figures 12 and 13, in the first half of the backhaul stage, piston acceleration is always positive. Thus, the velocity steadily increases. When the acceleration reaches zero, the maximum velocity is measured at 4.6 m/s. Piston acceleration in the second half of the backhaul stage is negative. The velocity begins to decrease, reducing to zero at the minimum value of top dead center acceleration. Acceleration starts in the first half of the strike stage. When it reaches zero, the velocity reaches its maximum value at 7.2 m/s. With gas entering the front chamber, the pressure of the back chamber rises, the acceleration is positive, and the velocity of the piston begins to

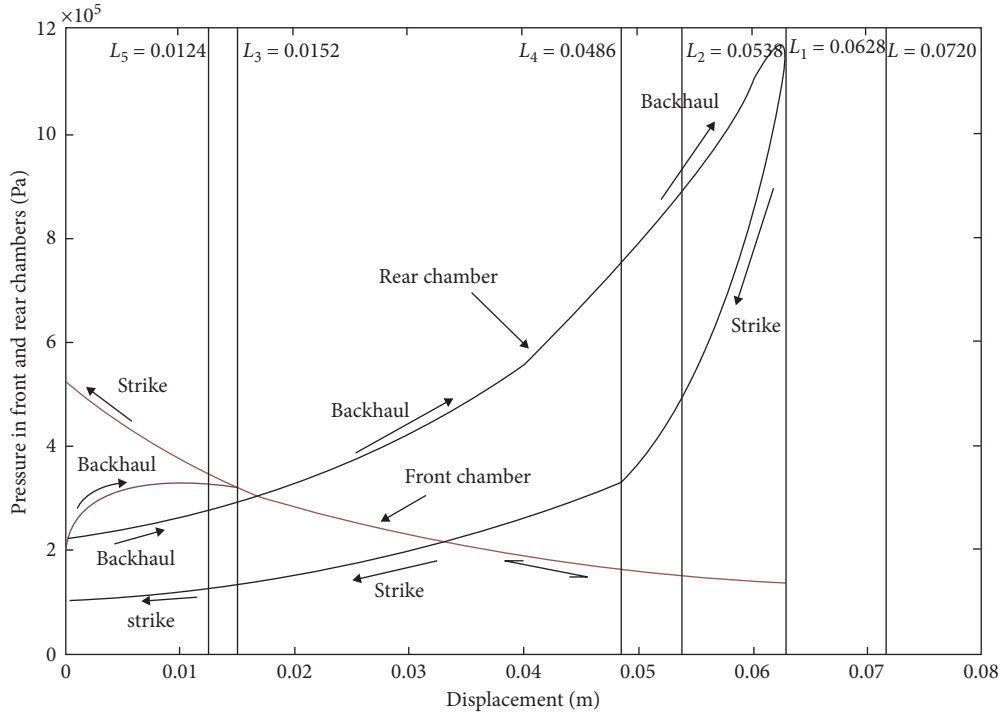

Figure 8: Pressure of the air in the front and rear chamber changes with displacement.

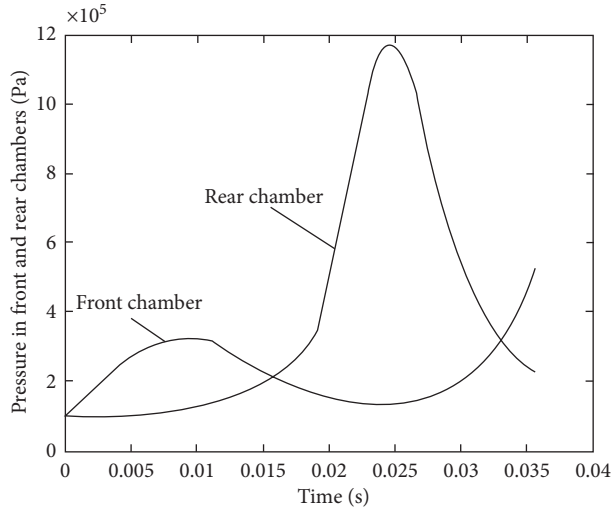

Figure 9: Pressure of the air in the front and rear chamber changes with time.

decline until it hits the bit at 6.2 m/s. Many signs are indicating that the piston stroke design is reasonable. The velocity curve directly and clearly describes the change of speed during the piston strike. The impact energy of the DTH hammer acts on the bit with the kinetic energy possessed by the piston. Only high-impact velocity can produce high-impact energy. The law and trend of velocity variation of the DTH hammer are analyzed through the velocity curve of the piston, and the internal parameters can be modified to realize the optimal design.

Based on the piston's acceleration and speed change curve, we can obtain the state parameters at any time step. Finally, frequency and air consumption can also be calculated. All of these parameters can be compared with those of other DTH hammers, and the credibility of the calculation can be verified.

As the deviation angle increases, the piston's acceleration will change during the whole circle, which will eventually lead to the decrease of the impact velocity of the piston. Due to the decline of impact velocity, the impact energy per blow

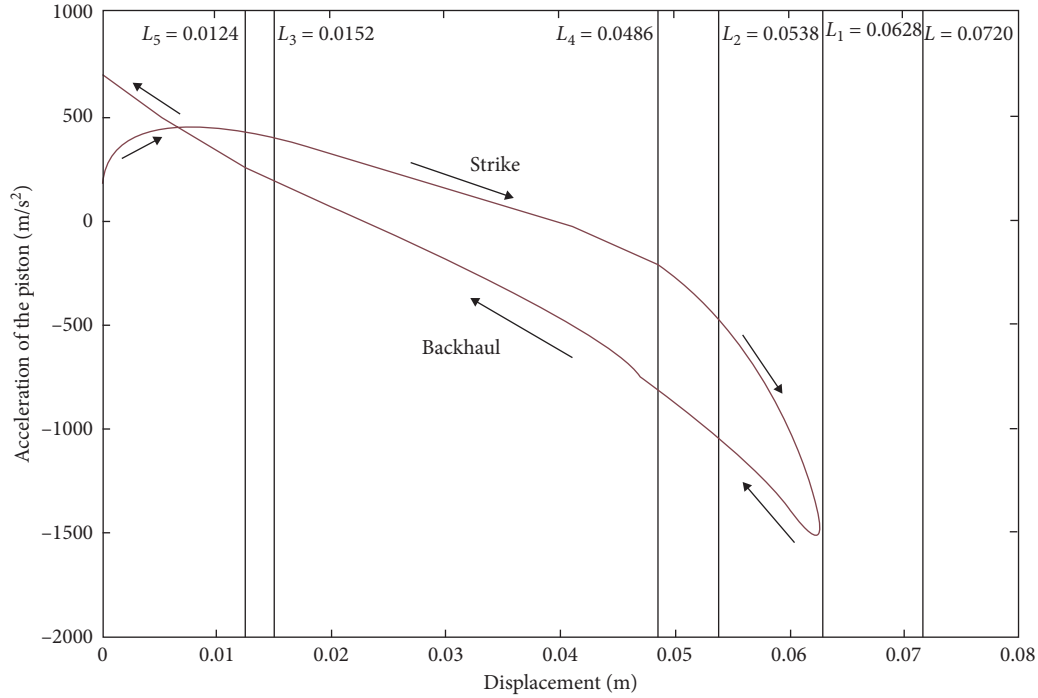

Figure 10: Acceleration curve of the piston changes with displacement.

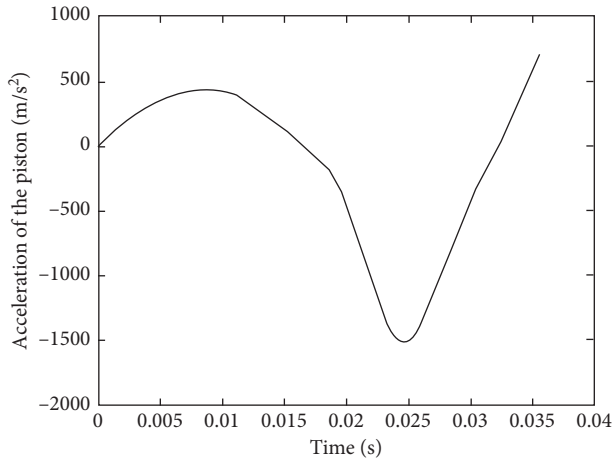

Figure 11: Acceleration curve of the piston changes with time.

in horizontal condition is 18.5% lower than in vertical condition, as shown in Figure 14, resulting in a decrease in the drilling rate and adequate power transferred to rock similar to the conventional hammers. However, the self-rotation motion of the novel hammer can reduce the friction force with the borehole, which will achieve better drilling efficiency in directional drilling.

Table 4 compares the proposed DTH hammer with conventional DTH hammers. The frequency of our hammer is slightly higher than that of similar-sized DTH hammers. Due to the considerable energy required by the piston to drive the spiral rod, ratchet wheel, hammer case, and drill bit, the air compressor needs relatively high pressure, and the air consumption is close to that of same-size conventional DTH hammers. The results show that the output energy of the novel DTH hammer is comparable to that of conventional DTH hammers, and the output of air compressor should be raised accordingly.

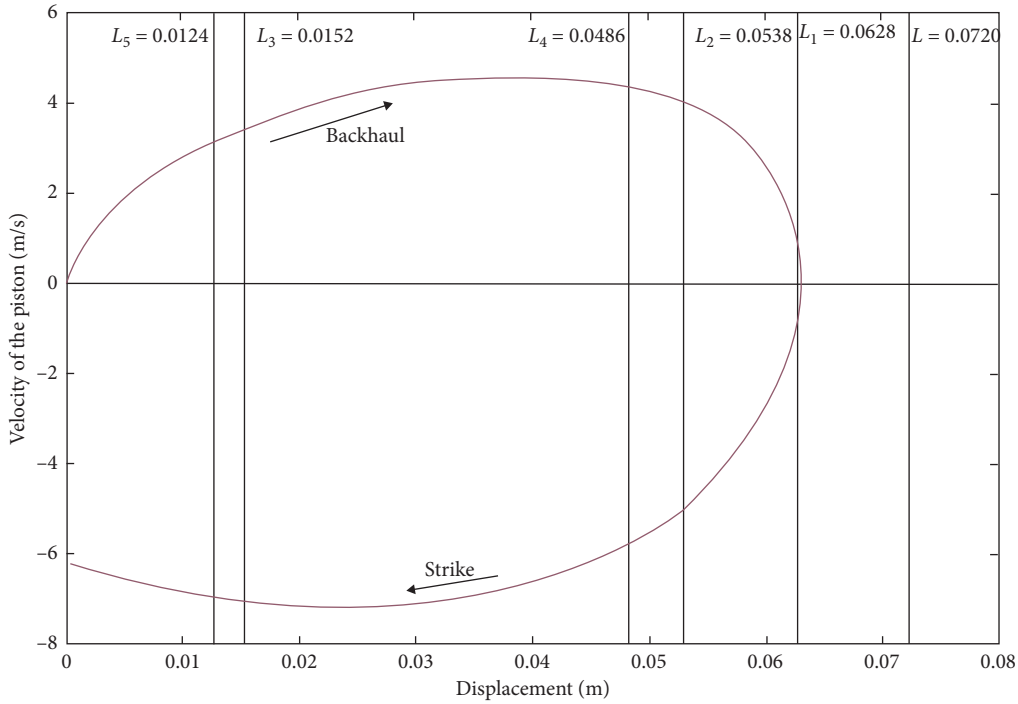

Figure 12: Impact velocity of the piston changes with displacement.

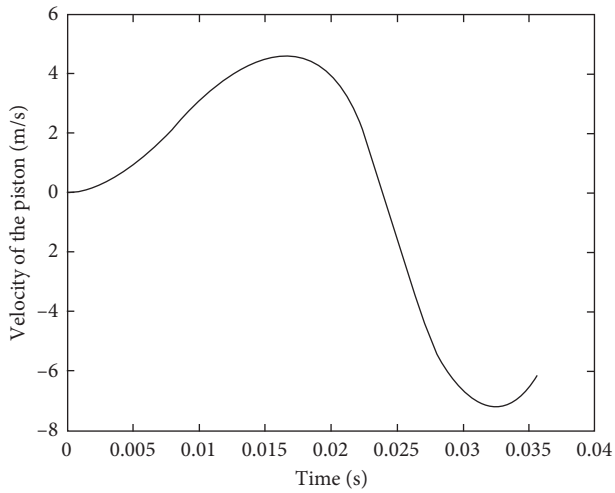

Figure 13: Impact velocity of the piston changes with time.

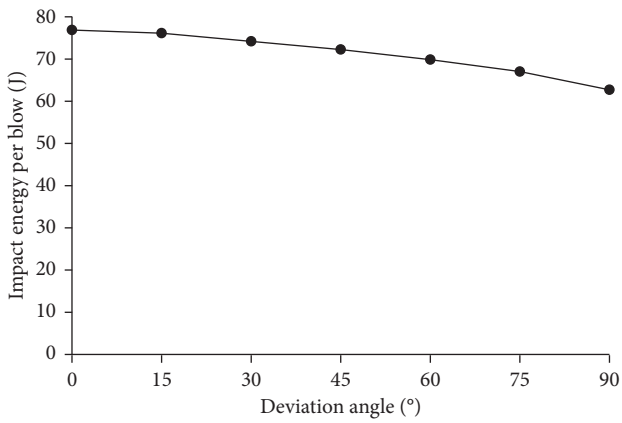

Figure 14: Impact energy per blow versus deviation angle.

Table 4: Technical parameters of the novel DTH hammer in comparison with other DTH hammers.

Type of DTH hammer	Novel hammer (Φ105 mm)	Valve hammer (Φ89 mm)	Valveless hammer (Φ89 mm)	RC hammer (Φ108 mm)	Rock drill (Φ75 mm)
Impact energy (J)	76	113	210	165	>70
Frequency (Hz)	28	16	19.2	18	>33
Pressure (MPa)	1.2	0.63	1.05	1.0	—
Air consumption (m^3/min)	3.18	9	4.5	5	<3.5

6. Conclusions

This paper defines and analyzes a novel pneumatic DTH hammer with a self-propelled round bit, where operating action is achieved through the interaction between the dynamical impact system and ratchet wheel mechanism. The proposed hammer has an improved structure compared to traditional DTH hammers. The ratchet wheel mechanism uses the energy of compressed air to realize the self-propelled rotating movement of the drill bit by converting the linear motion of the piston into the rotary motion of the DTH hammer.

The contributions of this paper can be summarized as follows:

(1) Following the above line of thinking, we present nonlinear dynamical modeling to assess the performance of the novel DTH hammer based on the finite-difference principle. The modeling couples the dynamic and kinematic modeling of the piston and the rotary mechanism, which can optimize the structural parameters of the DTH hammer, such as impact frequency, impact energy, piston motion, and air consumption. The nonlinear modeling approach allows the calculation of structural parameters to achieve an optimal design.

(2) The advanced engineering software MATLAB is used to simulate the working principle of the novel DTH hammer. According to the calculation results, a curve is drawn reflecting the piston motion process, which directly and clearly describes the pressure changes in the front and rear air chambers, the movement speed and acceleration of the piston, and the changing trend of air consumption during a working cycle. The simulation results indicate that the structural parameters of the DTH hammer with a self-propelled round bit are reasonable, and the design scheme is feasible. At the end of the strike, the piston's velocity is about 6 m/s, the impact of energy is 76 J, and the frequency is 28 Hz. The maximum air consumption of the system is 3.18 m^3/min, and the maximum velocity of the piston in the backhaul stage is 4.6 m/s.

(3) A validation experiment of the novel hammer is executed on the hammer test device, and the design principle and theory indicate feasibility. Since some hypotheses and factors are omitted in the mathematical modeling, such as friction force and heat exchange, the simulation results are markedly more considerable than the experimental data. Nonetheless, after further structural optimization, the DHT hammer with a self-propelled round bit will be capable of effectively reducing friction in directional drilling.

Data Availability

Some or all data, models, or code generated or used during the study are available from the corresponding author upon request.

Conflicts of Interest

The authors declare no conflicts of interest.

Acknowledgments

This work was financially supported by the National Key Research and Development Program of China (no. 2018YFC1505303) and Science and Technology Research and Planning Project of Jilin Provincial Education Department during the 13th Five-Year Plan (no. JJKH20190132KJ).

References

[1] S. Kahraman, N. Bilgin, and C. Feridunoglu, "Dominant rock properties affecting the penetration rate of percussive drills," *International Journal of Rock Mechanics and Mining Sciences*, vol. 40, no. 5, pp. 711–723, 2003.

[2] K. Bo, K. Yin, and J. M. Peng, "Reverse circulation DTH hammer drilling technique," *Global Geology*, vol. 14, no. 4, pp. 259–264, 2011.

[3] A. D. Batako, V. I. Babitsky, and N. A. Halliwell, "A self-excited system for percussive-rotary drilling," *Journal of Sound and Vibration*, vol. 259, no. 1, pp. 97–118, 2003.

[4] R. M. Wolke, K. Deakins, and R. L. Suter, "Air drilling techniques," *Geothermal Resources Council-Bulletin*, vol. 19, no. 5, pp. 138–143, 1990.

[5] B. Lundberg and M. Okrouhlik, "Efficiency of a percussive rock drilling process with consideration of wave energy radiation into the rock," *International Journal of Impact Engineering*, vol. 32, no. 10, pp. 1573–1583, 2005.

[6] M. S. Bruno, *Fundamental Research on Percussion Drilling: Improved Rock Mechanics Analysis, Advanced Simulation Technology, and Full-Scale Laboratory Investigations*, Terralog Technologies Inc., Calgary, Canada, 2005.

[7] National Research Council, *Drilling and Excavation Technologies for the Future*, National Academy Press, Washington, DC, USA, 1994.

[8] S. Ryu, J.-W. Cho, J.-Y. Park et al., "Optimum operating conditions of a multi-hammer drilling machine assessed using a linear percussion test," *International Journal of Precision Engineering and Manufacturing*, vol. 16, no. 7, pp. 1415–1422, 2015.

[9] C. G. Bu, X. F. Li, L. Sun et al., "Arithmetic solution for the axial vibration of drill string coupling with a down-the-hole hammer in rock drilling," *Journal of Vibration and Control*, vol. 22, no. 12, pp. 2090–3101, 2016.

[10] C. Bu, Y. Qu, Z. Cheng, and B. Liu, "Numerical simulation of impact on pneumatic DTH hammer percussive drilling," *Journal of Earth Sciences*, vol. 20, no. 5, pp. 868–878, 2009.

[11] A. Depouhon, V. Denoël, and E. Detournay, "Numerical simulation of percussive drilling," *International Journal for Numerical and Analytical Methods in Geomechanics*, vol. 39, no. 8, pp. 889–912, 2015.

[12] A. Depouhon, V. Denoël, and E. Detournay, "A drifting impact oscillator with periodic impulsive loading: application to percussive drilling," *Physica D: Nonlinear Phenomena*, vol. 258, pp. 1–10, 2013.

[13] L. E. Chiang and E. B. Stamm, "Design optimization of valveless DTH pneumatic hammers by a weighted pseudo-gradient search method," *Journal of Mechanical Design*, vol. 120, no. 4, pp. 687–694, 1998.

[14] V. A. Eremenko, V. N. Karpov, V. V. Timonin et al., "Basic trends in development of drilling equipment for ore mining with block caving method," *Journal of Mining Science*, vol. 51, no. 6, pp. 1113–1125, 2005.

[15] D.-J. Kim, J.-Y. Oh, J.-W. Cho, J. Kim, J. Chung, and C. Song, "Design study of impact performance of a DTH hammer using PQRSM and numerical simulation," *Journal of Mechanical Science and Technology*, vol. 33, no. 11, pp. 5589–5602, 2019.

[16] D. Kim, J. Kim, C. Song et al., "Prediction model of drilling performance for percussive rock drilling tool," *Advances in Civil Engineering*, vol. 2020, Article ID 8865684, 13 pages, 2020.

[17] Z. Zhao, Y. Meng, Y. Li, X. Shi, and C. Xiang, "Effects of working angle on pneumatic down-the-hole hammer drilling," *Rock Mechanics and Rock Engineering*, vol. 48, no. 5, pp. 2141–2155, 2015.

[18] V. I. Klishin, V. Timonin, D. I. Kokoulin, S. E. Alekseev, and B. Kubanychbek, "Enhancing down-the-hole air hammer capacity in directional drilling," *IOP Conference Series: Earth and Environmental Science*, vol. 84, Article ID 012020, 2017.

[19] Q. Liu, T. Yang, D. G. Wang et al., "Numerical simulation on the impact dynamics of a novel rotation air hammer and experimental research," *Journal of Vibroengineering*, vol. 17, no. 5, pp. 2260–2271, 2015.

[20] C. He, L. X. Han, X. B. Chen, and L. Chen, "Development of air hammer with self-propelled round bit and the contact analysis of the key components," *Advanced Materials Research*, vol. 339, pp. 243–249, 2011.

[21] Y. Hu, "Study on DTH with self-propelled round bit and its simulation analysis," Doctoral thesis, Jilin University, Changchun, China, 2007.

[22] X. Zhang, Y. Luo, L. Fan, J. Peng, and K. Yin, "Investigation of RC-DTH air hammer performance using CFD approach with dynamic mesh method," *Journal of Advanced Research*, vol. 18, pp. 127–135, 2019.

[23] T. Wu, Y. Tang, S. Tang et al., "Design and analysis of a new down-the-hole electromagnetic hammer driven by tube linear motor," *IET Electric Power Applications*, vol. 11, no. 9, pp. 558–1565, 2017.

[24] H. Fattahi and H. Bazdar, "Applying improved artificial neural network models to evaluate drilling rate index," *Tunnelling and Underground Space Technology*, vol. 70, pp. 114–124, 2017.

[25] S.-y. Yang, Y.-b. Ou, Y. Guo, and X.-m. Wu, "Analysis and optimization of the working parameters of the impact mechanism of hydraulic rock drill based on a numerical simulation," *International Journal of Precision Engineering and Manufacturing*, vol. 18, no. 7, pp. 971–977, 2017.